Available online at www.sciencedirect.com
ScienceDirect
Applied Catalysis B: Environmental 82 (2008) 67–76
APPLIED CATALYSIS B: ENVIRONMENTAL
www.elsevier.com/locate/apcatb

Kinetic study of photo-oxidation of NH_3 over TiO_2

Seiji Yamazoe, Yutaka Hitomi, Tetsuya Shishido, Tsunehiro Tanaka *

Department of Molecular Engineering, Graduate School of Engineering, Kyoto University, Kyoto 615-8510, Japan

Received 30 October 2007; received in revised form 19 December 2007; accepted 19 December 2007
Available online 11 January 2008

Abstract

Kinetic study was carried out for photo-oxidation of NH_3 (photo-SCO: $4NH_3 + 3O_2 \rightarrow 2N_2 + 6H_2O$) to elucidate the mechanisms of the photo-SCO over anatase and rutile TiO_2. The reaction orders of the reactant gases reveal that the photo-SCO activity depends only on the concentration of O_2 with either anatase or rutile TiO_2. Steady-state kinetics suggests that the rate-determining step is the formation of nitrosoamide species from surface NO species and NH_2 radical. The surface NO species may play an important role in the high activity of the photo-SCO. O_3 anion radical, which is a strong oxidant, was detected only over anatase TiO_2 and the concentration of surface NO species would be increased by O_3 anion radical. This may be the reason why anatase TiO_2 shows higher activity than rutile TiO_2. The photo-SCO activity is enhanced as the reaction temperature increased. 100% NH_3 conversion and 94% N_2 selectivity were achieved at GHSV = 50,000 h^{-1} at 435 K. This enhancement of the activity at higher reaction temperature is caused by (1) the increase in the surface NO species and (2) the improvement of reactivity between surface NO and NH_2 radical. The SCO activity is moderately high even at low temperature: the Arrhenius activation energy is only 24.4 kJ mol^{-1}.

Keywords: Ammonia oxidation; Kinetics; TiO_2; Photocatalyst; SCO

1. Introduction

It is desirable to remove ammonia from exhaust gas and/or waste water in industrial emission source in an environmental point of view. Ammonia can be eliminated by biological treatment, thermal combustion and catalytic oxidation. Recently, selective catalytic oxidation (SCO) of ammonia to nitrogen in the presence of excess oxygen has received much attention because this technique is promising for efficient removal of ammonia from exhaust gas [1–6]. The reaction stoichiometry in the typical SCO condition had been proposed as follows [7–12]:

$$4NH_3 + 3O_2 \rightarrow 2N_2 + 6H_2O \quad (1)$$

The SCO process may be applied to remove unreacted ammonia in the selective catalytic reduction (SCR) of NO with ammonia process [13,14]. In the case of the SCO process located at the downstream of the SCR process, the low-temperature operation of the SCO is often required. Therefore, many efforts have been made in order to develop the low-temperature SCO. Long and Yang reported that Cu- and Fe-exchanged ZSM-5 exhibited a good SCO activity at 623 K [1]. Gang et al. reported that Ag/Al_2O_3 showed high activity in the SCO in the range of >433 K [3]. A number of the other catalysts, such as CuO/Al_2O_3 [14,15], V_2O_5/TiO_2 [16], Pt-, Pd- and Rh-exchanged ZSM-5 [17], showed SCO activity. However, the aforementioned catalysts need high temperature (>433 K) in the SCO reaction.

Some kinetic studies of the SCO reaction over metal oxides have been reported in order to determine the rate-determining step and the activation energy [10,18–20]. Eqs. (2)–(5) are the most probable SCO reaction mechanism over metal oxide catalysts [10,14,19–22].

$$NH_3\,(+O) \rightarrow NH_2 + e^- + H^+\,(O) \quad (2)$$

$$NH_2 + O_2 \rightarrow NO + H_2O \quad (3)$$

$$NH_2 + NO \rightarrow NH_2NO \quad (4)$$

$$NH_2NO \rightarrow N_2 + H_2O \quad (5)$$

It has been proposed that the rate-determining step of the SCO over metal oxide catalysts is Eq. (2) (NH_3 activation process) [10,18–20]. Additionally, activation energy (E_a) of

* Corresponding author. Tel.: +81 75 383 2558; fax: +81 75 383 2561.
E-mail address: tanakat@moleng.kyoto-u.ac.jp (T. Tanaka).

0926-3373/$ – see front matter
doi:10.1016/j.apcatb.2007.12.023

Nomenclature

r	N_2 production rate (mol s^{-1})
k	rate constant
C_{NH_3}	concentration of NH_3 (mol L^{-1})
C_{O_2}	concentration of O_2 (mol L^{-1})
α	reaction order of NH_3
β	reaction order of O_2
$k_{\pm i}$	rate constant at Step i
K_i	equilibrium constant at Step i
S	Lewis acid site on TiO_2
S^-	reduced Lewis acid site
$O^{2-}_{lattice}$	lattice oxygen
$[S]_0$	total amount of Lewis acid site on TiO_2 (mol L^{-1})
$[NH_2^{\bullet}–S]$	concentration of $NH_2^{\bullet}$–S species (mol L^{-1})
$[NO–S^-]$	concentration of NO–S^- species (mol L^{-1})
$[O_2]$	concentration of O_2 ($= C_{O_2}$) (mol L^{-1})
T	reaction temperature (K)

the SCO reaction is high (76–139 kJ mol^{-1}) [18–20]. These results indicate that the SCO of ammonia at low temperature is difficult due to the high E_a of NH_3 activation. Therefore, a development of new SCO system with low E_a of NH_3 activation is required.

Cant and Cole reported that the SCO reaction was carried out in a closed system over TiO_2 photocatalyst under irradiation (photo-SCO) at room temperature although the activity was low [23]. Recently, we have reported that the photo-SCO proceeds with high activity (NH_3 conversion: 100%, N_2 selectivity: 84% at gas hourly space velocity (GHSV) = 25,000 h^{-1}) at room temperature over TiO_2 in a fixed bed flow system [24]. The photo-SCO reaction stoichiometry is same as that in the conventional SCO (Eq. (1)). The reaction mechanism of the photo-SCO over TiO_2 was elucidated by UV–vis, electron spin resonance (ESR) and Fourier transform infrared (FT-IR) spectroscopies and determined as shown in Scheme 1 [24,25]. Our proposed reaction mechanism is almost similar to the conventional SCO reaction mechanism. NH_3 is adsorbed to Lewis acid site of TiO_2 in the dark (Step 1). Adsorbed NH_3 is activated to NH_2 radical by trapping a photo-formed hole and a photo-formed electron reduces Ti^{4+} site to Ti^{3+}. O_2 reacts with an electron or a hole, which are formed under UV irradiation, to form oxygen anion radical species ($O_2^{\bullet-}$ or $O_3^{\bullet-}$) (Step 3). NH_2 radical reacts with oxygen anion radical species to form NO without light (Step 4). The NO reacts with NH_2 radical and NH_2NO species is generated as an intermediate (Step 5). The NH_2NO species is decomposed to N_2 and H_2O (Step 6). Finally, the reduced Ti^{3+} is re-oxidized by the reaction with O_2 (Step 7). Additionally, we found that the crystal phase of TiO_2 affects the types of oxygen anion radical [24]. Rutile TiO_2 generates only O_2 anion radical whereas anatase TiO_2 forms not only O_2 anion radical but also O_3 anion radical. The catalytic activities of various TiO_2 in the photo-SCO reaction indicate that O_3 anion radical plays a key role in the higher activity than O_2 anion radical.

The photo-SCO proceeds even at room temperature, since the activation of NH_3 proceeds at room temperature by photo-excitation (Step 2). Thus, the rate-determining step of the photo-SCO is different from the conventional SCO reaction and the activation energy of the photo-SCO is expected to be lower than that of the conventional SCO. In this study, we carried out the kinetic study of the photo-SCO over TiO_2 using steady-state approximation not only to determine the rate-determining step of the photo-SCO reaction but also to clarify the reaction mechanism as shown in Scheme 1. The thermal effect for the photo-SCO was also investigated. Furthermore, we discussed the reactivity of O_3 and O_2 anion radical species in terms of kinetics.

2. Experimental

2.1. Preparation and characterization of catalysts

Two kinds of TiO_2 (JRC-TIO-3 and JRC-TIO-8 supplied from the Japan Catalysis Society) were hydrated in distilled water for 2 h at 353 K, followed by filtration with suction pump. The sample was dried at 383 K overnight, followed by calcination in dry air at 673 K for 3 h. After the hydration and calcinaton described above, JRC-TIO-3 and JRC-TIO-8 were used in this study.

The specific surface area of the prepared JRC-TIO-3 and JRC-TIO-8 were evaluated to be 46 and 93 $m^2\ g^{-1}$ by the BET method using N_2 adsorption isotherm at 77 K. We confirmed that the prepared JRC-TIO-3 and JRC-TIO-8 consist of rutile and anatase phases respectively by the XRD patterns. Amount of acid sites on TiO_2 was determined by the adsorption equilibrium method of NH_3 according to the previous work [24,26]. Before the adsorption equilibrium method, TiO_2 was evacuated at 673 K as a pretreatment.

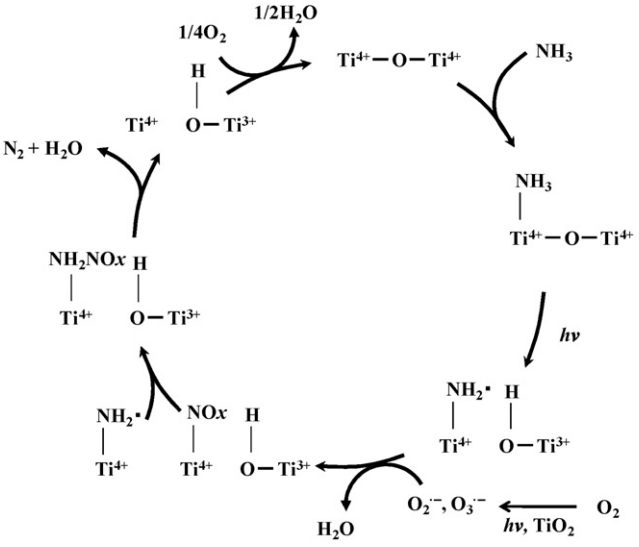

Scheme 1. Proposed reaction mechanism of photo-SCO.

2.2. Catalytic reaction

Photo-SCO was carried out in a conventional fixed bed flow system at an atmospheric pressure and at room temperature. Catalysts were fixed with quartz wool and filled up in a Pyrex reactor which has flat facets (12 mm × 10 mm × 1 mm). Before reactions, catalysts were pretreated at 673 K by flowing 10% O_2 diluted with Ar at 50 mL min^{-1} for 1 h. The typical reaction gas composition was as follows: NH_3 1000 ppm, O_2 2%, Ar balance. A PerkinElmer PE300BF 300 W Xe lamp was used as a light source and samples were irradiated from the one side of the flat facets of the reactor. N_2 and N_2O products were analyzed by a SHIMADSU GC-8A TCD gas chromatograph with MS-5A column for N_2 detection and Porapak Q for N_2O. The quantity of produced NO*x* (NO and NO_2) was determined by a Shimadzu NOA-7000 NO*x* analyzer.

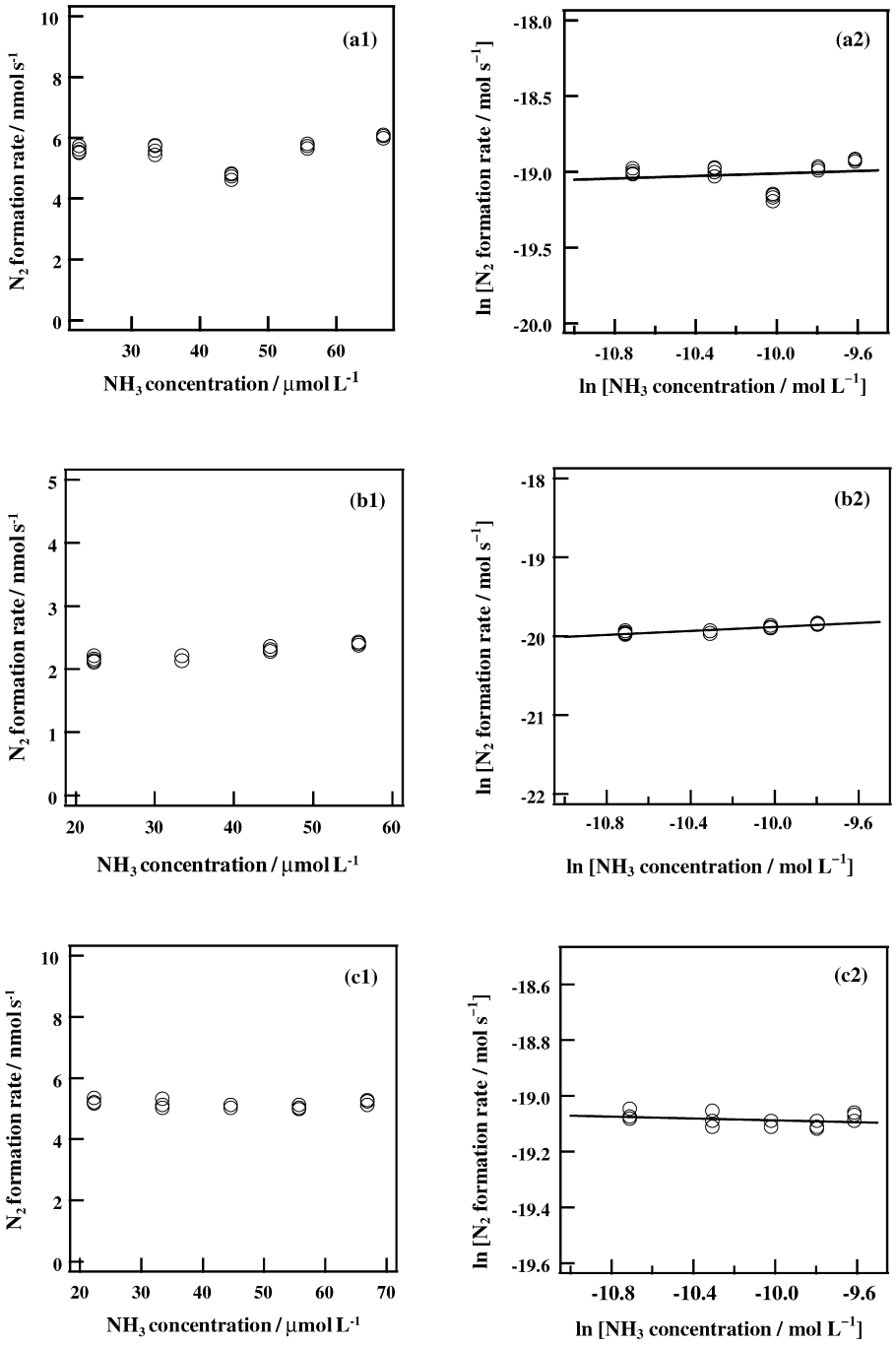

Fig. 1. N_2 formation rate in the photo-SCO (a1) over JRC-TIO-8 at 298 K, (b1) over JRC-TIO-3 at 298 K and (c1) over JRC-TIO-8 at 388 K under condition of various NH_3 concentrations (500–1500 ppm = 2.23×10^{-5} to 6.69×10^{-5} mol L^{-1}) (○). (a2), (b2) and (c2) show logarithms of (a1), (b1) and (c1) (○) and the approximate lines appeared at Eqs. (7), (30) and (37) (line), respectively.

2.3. Kinetics measurements

Kinetics measurements of the photo-SCO were carried out in a conventional fixed bed flow system at an atmospheric pressure and at room temperature. Catalyst was fixed with quartz wool and a given amount of catalyst was packed in a reactor to put a differential condition into practice. Catalysts were pretreated at 673 K by flowing 10% O_2 diluted with Ar at 50 mL min^{-1} for 1 h. The concentration of NH_3 and O_2 was converted at 500–1500 ppm or 1–3%, respectively. In this kinetic study, the photo-SCO reaction took place under the constant light intensity. Accordingly, the logarithms of the N_2 production rate were plotted and approximated by a straight line to determine the reaction orders.

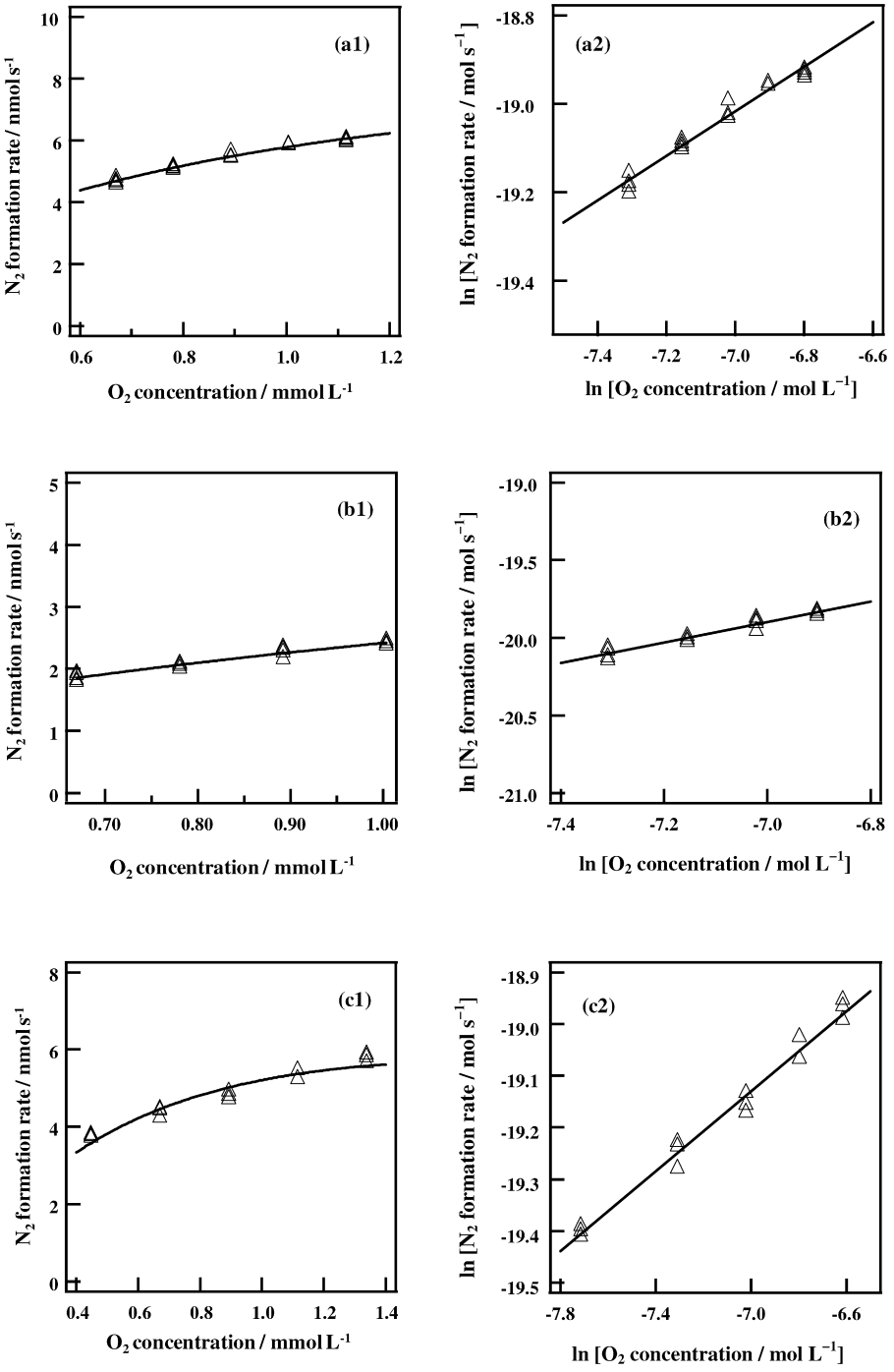

Fig. 2. N_2 formation rate in the photo-SCO (a1) over JRC-TIO-8 at 298 K, (b1) over JRC-TIO-3 at 298 K and (c1) over JRC-TIO-8 at 388 K under condition of various O_2 concentrations (1.5–2.5% = 6.69×10^{-4} to 1.12×10^{-3} mol L^{-1}) (Δ) and the approximate curve derived from Eq. (21) and Table 1 (line). (a2), (b2) and (c2) show logarithms of (a1), (b1) and (c1) (Δ) and the approximate lines appeared at Eqs. (8), (31) and (38) (line), respectively.

3. Results and discussion

3.1. Kinetic study of the photo-SCO over anatase TiO_2

It can be thought that the photo-SCO reaction rate depends on the concentrations of NH_3 and O_2 and light intensity. In the photo-SCO reaction condition, the alternation of the light intensity slightly affects the reaction temperature because a part of the light energy converts to thermal energy [27]. In this study, the photo-SCO reaction was carried out under the constant light intensity in order to ignore the factor of the thermal contribution to the photo-SCO activity, due to the change of the light intensity. Thus, the photo-SCO reaction rate under the constant light intensity is expressed as a following formula:

$$r = kC_{NH_3}^{\alpha} C_{O_2}^{\beta} \tag{6}$$

Figs. 1(a1) and 2(a1) show the N_2 formation rate in the photo-SCO over JRC-TIO-8 (anatase TiO_2) under the condition of various concentrations of NH_3 and O_2, respectively. The logarithmic plots of Figs. 1(a1) and 2(a1) are shown in Figs. 1(a2) and 2(a2), respectively. These logarithmic plots can be reasonably fitted with by a straight line shown in Figs. 1(a2) and 2(a2). These lines are expressed as following equations:

$$\ln r = -18.6(\pm 0.5) + 0.04(\pm 0.05) \ln C_{NH_3} \tag{7}$$

$$\ln r = -15.5(\pm 0.1) + 0.50(\pm 0.02) \ln C_{O_2} \tag{8}$$

Eqs. (6)–(8) show that the reaction orders of NH_3 and O_2 were close to zero and 0.5th order. The reaction orders of NH_3 and O_2 indicate that the rate-determining step of the photo-SCO over anatase TiO_2 would be the reaction process involving O_2 (Steps 3 or 7) or products generated by the reaction of O_2 (Steps 4, 5 or 6). The value of k is estimated at $e^{-15.5(\pm 0.1)}$ from Eqs. (6) and (8). This value is close to that obtained from Eqs. (6) and (7) ($k = e^{-15.1(\pm 0.5)}$), where $C_{O_2} = 8.90 \times 10^{-4}$ mol L^{-1} and $\beta = 0.5$ were used. According to the above results, the reaction rate is expressed as follows:

$$r = e^{-15.5(\pm 0.1)} \times C_{NH_3}^{0} C_{O_2}^{0.5} \tag{9}$$

In order to verify our proposed reaction mechanism (Scheme 1) and to determine the rate-determining step of the photo-SCO, the obtained rate equation (Eq. (9)) is compared with the rate equation derived from our proposed reaction mechanism. Rate constants and equilibrium constants in each elementary step are defined as follows:

$$\text{Step 1} \quad NH_3 + S \underset{k_{-1}}{\overset{k_1}{\rightleftarrows}} NH_3{-}S \quad K_1 = \frac{k}{k_{-1}} \tag{10}$$

$$\text{Step 2} \quad NH_3{-}S \underset{k_{-2}}{\overset{k_2}{\rightleftarrows}} NH_2^{\bullet}{-}S + H^+ \quad K_2 = \frac{k_2}{k_{-2}} \tag{11}$$

$$\text{Step 3} \quad O_2(+O_{lattice}^{2-}) \underset{k_{-3}}{\overset{k_3}{\rightleftarrows}} O_2^{\bullet -}(+O_3^{\bullet -}) \quad K_3 = \frac{k_3}{k_{-3}} \tag{12}$$

Step 4

$$NH_2^{\bullet}{-}S + O_2^{\bullet -}(\text{or } O_3^{\bullet -}) \underset{k_{-4}}{\overset{k_4}{\rightleftarrows}} NO{-}S^- + H_2O(+O_{lattice})$$

$$K_4 = \frac{k_4}{k_{-4}} \tag{13}$$

$$\text{Step 5} \quad NO{-}S^- + NH_2^{\bullet}{-}S \underset{k_{-5}}{\overset{k_5}{\rightleftarrows}} NH_2NO{-}S^- + S \tag{14}$$

$$K_5 = \frac{k_5}{k_{-5}}$$

$$\text{Step 6} \quad NH_2NO{-}S^- \underset{k_{-6}}{\overset{k_6}{\rightleftarrows}} N_2 + H_2O + S^- \quad K_6 = \frac{k_6}{k_{-6}} \tag{15}$$

$$\text{Step 7} \quad S^- + \tfrac{1}{4}O_2 + H^+ \underset{k_{-7}}{\overset{k_7}{\rightleftarrows}} S^- + \tfrac{1}{2}H_2O \quad K_7 = \frac{k_7}{k_{-7}} \tag{16}$$

We reported that Steps 2 and 3 proceed by photo-irradiation [25]. In Step 3, $O_2^{\bullet -}$ is generated by the reaction of O_2 with photo-formed electron and $O_3^{\bullet -}$ is produced by the reaction of O_2 with lattice oxygen and photo-formed hole [24,28–30]. We derived the following rate equation by assuming that each step is rate-determining step:

$$r = \frac{k_1 K_3^{1/2} K_4^{1/2} K_5^{1/2} K_6 K_7 [S]_0 C_{NH_3} C_{O_2}^{1/4}}{k_1 K_3^{1/2} K_4^{1/2} K_5^{1/2} K_6 K_7 C_{O_2}^{1/4} + K_6^{1/2} + K_3 K_4 K_6^{1/2} C_{O_2} + K_3^{1/2} K_4^{1/2} K_5^{1/2}(1 + K_6)} \quad (\text{Step 1}) \tag{17}$$

$$r = k_2 [S]_0 \quad (K_1 \gg 1) \quad (\text{Step 2}) \tag{18}$$

$$r = k_3 [S]_0 C_{O_2} \quad (\text{Step 3}) \tag{19}$$

$$r = \frac{k_4 K_2 K_3 [S]_0 C_{O_2}}{1 + K_2} \quad (K_1 \gg 1) \quad (\text{Step 4}) \tag{20}$$

$$r = \frac{k_5 K_2^2 K_3 K_4 [S]_0^2 C_{O_2}}{(1 + K_2 + K_2 K_3 K_4 C_{O_2})^2} \quad (K_1 \gg 1) \quad (\text{Step 5}) \tag{21}$$

$$r = k_6 [S]_0 \quad (K_1 \gg 1) \quad (\text{Step 6}) \tag{22}$$

$$r = \frac{k_7 K_2 [S]_0 C_{O_2}^{3/4}}{1 + K_2 + K_2 K_3 K_4 C_{O_2} + K_2 K_3^{1/2} K_4^{1/2} K_5^{1/2} K_6^{-1/2}(1 + K_6) C_{O_2}^{1/2}} \quad (K_1 \gg 1) \quad (\text{Step 7}) \tag{23}$$

In Step 2 and Steps 4–7, approximation of $K_1 \gg 1$ was used because NH_3 is adsorbed on the Lewis acid site strongly. The reaction orders of NH_3 and O_2 in the Steps 1–4 and 6 do not satisfy Eq. (9). Consequently, Step 5 (Eq. (21)) or Step 7 (Eq. (23)) is the rate-determining step of the photo-SCO. To determine which step is the rate-determining step, the experimental result was fitted with Eqs. (21) or (23).

Eq. (23) can be transformed as follows:

$$\frac{C_{O_2}^{3/4}}{r} = \frac{1}{k_7 K_2 [S]_0}[K_2 K_3 K_4 (C_{O_2}^{1/2})^2 + K_2 K_3^{1/2} K_4^{1/2} K_5^{1/2} K_6^{-1/2}(1+K_6) C_{O_2}^{1/2} + 1 + K_2] \quad (24)$$

$C_{O_2}^{3/4}/r$ obtained from Fig. 2a could not be fitted with Eq. (24). Eq. (21) is transformed as follows:

$$\left[\frac{C_{O_2}}{r}\right]^{1/2} = \frac{1}{(k_5 K_2^2 K_3 K_4 [S]_0^2)^{1/2}}(K_2 K_3 K_4 C_{O_2} + 1 + K_2) \quad (25)$$

Fig. 3(a) shows the plot of $(C_{O_2}/r)^{1/2}$ against C_{O_2} using the data of Fig. 2(a1). $(C_{O_2}/r)^{1/2}$ exhibited a good linear correlation with C_{O_2} and the fitted line shown in Fig. 3(a) is expressed as follows:

$$\left(\frac{C_{O_2}}{r}\right)^{1/2} = 1.2(\pm 0.04) \times 10^5 \times C_{O_2} + 300(\pm 4) \quad (26)$$

Thus, we determined that the rate-determining step of the photo-SCO over anatase TiO_2 is the process of the reaction of NH_2 radical with the formed NO species because the dependency of N_2 formation rate on O_2 concentration is interpreted only by Eq. (21). The following relation was derived from Eqs. (25) and (26).

$$\frac{K_2 K_3 K_4}{1 + K_2} = 380(\pm 20) \quad (27)$$

In our previous study, we reported that the lifetime of NH_2 radical is very long and the value of k_{-2} is $1.2 \times 10^{-2}\ s^{-1}$[31]. The rate of charge separation was reported to be 10^8–$10^{13}\ s^{-1}$ in dye-sensitized TiO_2 and artificial photosynthetic systems [32–34]. Applying this value for our system, the value of $K_2 = 10^{10}$–10^{15} would be very large. Therefore, Eq. (27) is simplified to the following equation.

$$K_3 K_4 = 380(\pm 20) \quad (28)$$

Substitution of Eq. (27) into Eq. (21) gives the following formula:

$$r = \frac{380 \times k_5 [S]_0^2 C_{O_2}}{[1 + 380 \times C_{O_2}]^2} \quad (29)$$

where, the approximation of $K_2 \gg 1$ is used. The dependency of N_2 formation rate on O_2 concentration in Fig. 2(a1) is reasonably fitted with Eq. (29) and the value of $k_5[S]_0^2 = 2.9(\pm 0.01) \times 10^{-8}\ mol\ s^{-1}$ is obtained. The value of $[S]_0$ of TiO_2 (JRC-TIO-8) is estimated at 0.37 mol L^{-1} (Lewis acid site amount of JRC-TIO-8: 400 μmol g^{-1}, catalyst amount used in this study: 0.11 g). These values are summarized in Table 1. Consequently, $k_5 = 2.1 \times 10^{-7}\ L^2\ mol^{-1}\ s^{-1}$ is obtained.

Eq. (21) could well account for the experimental results in Fig. 2(a1). The N_2 formation rate of the photo-SCO over anatase TiO_2 (JRC-TIO-8) is expressed by Eq. (29). The correspondence of the experimental results with the calculation results as shown in Figs. 2(a1) and 3(a) indicates that the proposed reaction mechanism photo-SCO (Scheme 1) is supported by the kinetic study. It is concluded that the rate-determining step of the photo-SCO is the reaction process of NH_2 radical with formed NO species (Step 5). Therefore, the higher surface concentrations of NH_2 radical and formed NO species would provide the higher photo-SCO activity. We have already reported that TiO_2 with the large amount of acid site and the high formation ability of oxygen anion radical species shows high photo-SCO activity. Since the large amount of acid site and the high formation ability of oxygen anion radical species lead to the increase in the amount of NH_2 radical and NO species, it is reasonable that the rate-determining step is Step 5. The values of k, K_3K_4 and k_5, listed in Table 1, are estimated from the kinetic analysis. There values are discussed below.

3.2. Kinetic study of the photo-SCO over rutile TiO_2

We reported that the reactivity of rutile TiO_2 is different from that of anatase in photo-SCO [24]. We also carried out the kinetic study of the photo-SCO at room temperature over rutile TiO_2. According to the kinetic analysis, the rate-determining step of the photo-SCO over rutile TiO_2 is the reaction of NH_2 radical with the formed NO species as well as anatase TiO_2. Figs. 1(b1, b2), 2(b1, b2), and 3(b) show the experimental results of the dependency of N_2 formation rate on NH_3 and O_2 concentrations, their logarithmic plots and the plot of $(C_{O_2}/r)^{1/2}$ against C_{O_2} using the data of Fig. 2(b1), respectively. The approximated lines of the data of Figs. 1(b2), 2(b2), and 3(b) are shown in Figs. 1(b2), 2(b2), and 3(b) and the obtained equations of these approximated lines are listed in Table 2. The rate equations over rutile TiO_2 calculated by Eqs. (30) and (31) are listed in Table 3. Additionally, the values of K_3K_4 and k_5 evaluated using Eqs. (25), (32) and $[S]_0 = 0.24$ mol L^{-1} (Lewis acid site amount of JRC-TIO-3: 180 μmol g^{-1}, the amount of this catalyst used in this study: 0.16 g) are shown in Table 1.

3.3. Comparison of the reactivity between anatase and rutile TiO_2

In this section, the difference in the reactivity between anatase (JRC-TIO-8) and rutile (JRC-TIO-3) TiO_2 is discussed based on the kinetic analysis. As the rate-determining step of the photo-SCO over both anatase and rutile TiO_2 is Step 5 (Eq. (14)), the reaction rate is expressed as follows:

$$r = k_5[NH_2^{\bullet}\text{–}S][NO\text{–}S^-] \quad (34)$$

The value of k_5 for anatase TiO_2 is almost as same as that for rutile TiO_2 (see Table 1). Therefore, the photo-SCO activity is proportional to both $[NH_2^{\bullet}\text{–}S]$ and $[NO\text{–}S^-]$. The values of $[NH_2^{\bullet}\text{–}S]$ and $[NO\text{–}S^-]$ can be estimated by Eq. (34) and the following equation:

$$K_3 K_4 = \frac{[NO\text{–}S^-]}{[NH_2^{\bullet}\text{–}S][O_2]} \quad (35)$$

Eq. (35) is obtained from Eqs. (12) and (13). $[NH_2^{\bullet}\text{–}S]$ and $[NO\text{–}S^-]$ were calculated by the substitution of r, k_5, K_3K_4 and

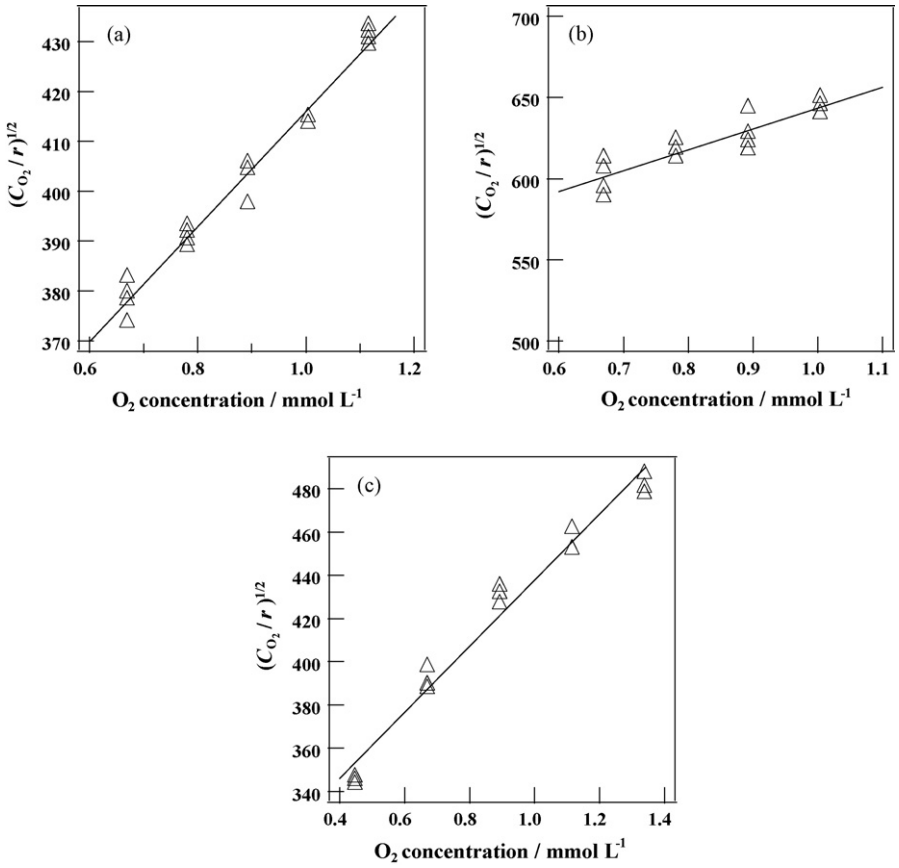

Fig. 3. (a–c) are the plots of $(C_{O_2}/r)^{1/2}$ against C_{O_2} (Δ) in the results of Fig. 2(a1), (b1) and (c1) and the approximate lines appeared at Eqs. (26), (32) and (39) (line), respectively.

$[O_2]$ into Eqs. (34) and (35). The obtained values of $[NH_2^{\bullet}–S]$ and $[NO–S^-]$ of anatase and rutile TiO_2 are listed in Table 1 (5.4×10^{-9} and 2.3×10^{-9} mol L^{-1} were used as the values of r of anatase and rutile TiO_2 under the reaction condition of NH_3 = 1000 ppm and O_2 = 2% (8.90×10^{-4} mol L^{-1}) in Fig. 2(a1) and (b1). In either case, $[NO–S^-]$ is lower than $[NH_2^{\bullet}–S]$. As the sum of $[NH_2^{\bullet}–S]$ and $[NO–S^-]$ is equal to the total amount of acid site ($[S]_0$) in the case of both anatase and rutile, the acid site on TiO_2 would be covered with NH_2 radical and NO species in the steady-state of the photo-SCO reaction. This result is reasonable because the rate-determining step is Eq (14). Additionally, Eq. (34) is transformed using $[S]_0 = [NH_2^{\bullet}–S] + [NO–S^-]$ as follows:

$$r = k_5[S]_0^2\left(\frac{1}{4} - \left(\frac{[NO^- - S]}{[S]_0} - \frac{1}{2}\right)\right)^2 \quad (36)$$

Eq. (36) clearly indicates that the photo-SCO shows the highest activity when the value of $[NO–S^-]/[S]_0$ is close to 0.5. The values of $[NO–S^-]/[S]_0$ of anatase and rutile are 0.26 and 0.18, respectively (Table 1), and $[NO–S^-]/[S]_0$ of anatase is closer to 0.5 than that of rutile. We reported that the reactivity of anatase TiO_2, which generates both O_2 and O_3 anion radical, was higher than that of rutile TiO_2, generating only O_2 anion radical (shown Fig. 7 in Ref. [24]). It is well known that O_3 anion radical has a higher oxidizability than O_2 anion radical [30,35]. This high oxidizability enhances the formation of $NO–S^-$ (Eq. (13)). Therefore, anatase exhibits larger value of $[NO–S^-]/[S]_0$ than rutile.

3.4. Development of the photo-SCO activity by the increase in the reaction temperature

It is expected that the photo-SCO activity is enhanced by the increase in the reaction temperature because the reactivity of

Table 1
Parameters obtained from the kinetic analysis

Catalyst	k_5 (L^2 mol^{-1} s^{-1})	K_3K_4 (L mol^{-1})	$[S]_0$[a] (mol L^{-1})	$[NH_2^{\bullet}–S]$ (mol L^{-1})	$[NO–S^-]$ (mol L^{-1})	$[NO–S^-]/[S]_0$
JRC-TIO-8 at RT[b]	2.1×10^{-7}	380(±20)	0.37	0.27	0.093	0.26
JRC-TIO-3 at RT[b]	2.6×10^{-7}	250(±30)	0.24	0.20	0.045	0.18
JRC-TIO-8 at 388 K[c]	1.0×10^{-6}	540(±40)	0.15	0.10	0.049	0.33

[a] Total amount of acid site on TiO_2 determined by NH_3 adsorption.
[b] The photo-SCO was carried out at room temperature under photo-irradiation.
[c] The photo-SCO was carried out at 388 K under photo-irradiation.

Table 2
Obtained approximate equations

Figure number	Formula
JRC-TIO-8 at RT[a]	
1b	$\ln r = -18.6(\pm0.5) + 0.04(\pm0.05)\ln C_{NH_3}$
2b	$\ln r = -15.5(\pm0.1) + 0.50(\pm0.02)\ln C_{O_2}$
3	$(C_{O_2}/r)^{1/2} = 1.2(\pm0.04) \times 10^5 \times C_{O_2} + 300(\pm4)$
JRC-TIO-3 at RT[a]	
4b	$\ln r = -18.7(\pm0.2) + 0.12(\pm0.02)\ln C_{NH_3}$
5b	$\ln r = -15.2(\pm0.3) + 0.66(\pm0.04)\ln C_{O_2}$
6	$(C_{O_2}/r)^{1/2} = 1.3(\pm0.16) \times 10^5 \times C_{O_2} + 510(\pm4)$
JRC-TIO-8 at 388 K[b]	
9b	$\ln r = -19.3(\pm0.2) + 0.02(\pm0.02)\ln C_{NH_3}$
10b	$\ln r = -16.4(\pm0.1) + 0.39(\pm0.01)\ln C_{O_2}$
11	$(C_{O_2}/r)^{1/2} = 1.5(\pm0.07) \times 10^5 \times C_{O_2} + 290(\pm7)$

[a] The photo-SCO was carried out at room temperature under photo-irradiation.
[b] The photo-SCO was carried out at 388 K under photo-irradiation.

surface species is enhanced by the development of their mobility. Fig. 4 shows the effect of the reaction temperature on N_2 formation rate. It is clearly shown that the increase in the reaction temperature enhanced the photo-SCO activity. The SCO reaction does not proceed without the photo-irradiation. These results indicate that the photo-irradiation is essential for the photo-SCO over TiO_2 and that the development of the photo-SCO activity would be caused by the enhancement of the rate of Step 5.

Fig. 5 shows the time course of the photo-SCO reaction over JRC-TIO-8 at 435 K. 100% NH_3 conversion and 94% N_2 selectivity were achieved at GHSV = 50,000 h^{-1}. By-products were N_2O (14 ppm) and NO*x* (33 ppm). We confirmed that the photo-SCO is the efficient reaction system even at low temperature.

3.5. Kinetic study of the photo-SCO over anatase TiO_2 at 388 K

The photo-SCO activity was enhanced by the increase in the reaction temperature. We also carried out the kinetic study of the photo-SCO over anatase TiO_2 at 388 K in order to clarify causes of the development of the activity. As a result of the kinetic analysis as well as anatase and rutile TiO_2 at room temperature, the rate-determining step of the photo-SCO at 388 K over anatase TiO_2 is also the process of the reaction of NH_2 radical with the formed NO species. Figs. 1(c1, c2), 2(c1, c2), and 3(c) show the experimental results of the dependency of N_2 formation rate on NH_3 and O_2 concentrations, their logarithmic plots and the plot of $(C_{O_2}/r)^{1/2}$ against C_{O_2} using the data of Fig. 2(c1), respectively. The approximated lines of the data in Figs. 1(c2), 2(c2), and 3(c) are shown in Figs. 1(c2), 2(c2), and 3(c) and the obtained equations of these approximated lines are listed in Table 2. The rate equation over anatase TiO_2 at 388 K calculated by Eqs. (37) and (38) is listed in Table 3. Moreover, the values of K_3K_4 and k_5 evaluated using Eqs. (25), (39) and $[S]_0 = 0.15$ mol L^{-1} (catalyst amount used in this study: 0.04 g) are shown in Table 1.

Table 3
Obtained rate equations

Catalyst	Rate equation
JRC-TIO-8 at RT[a]	$r = e^{-15.5(\pm0.1)} \times C^0 C_{O_2}^{0.5}$
JRC-TIO-3 at RT[a]	$r = e^{-14.2(\pm0.3)} \times C^{0.1} C_{O_2}^{0.7}$
JRC-TIO-8 at 388 K[b]	$r = e^{-16.4(\pm0.1)} \times C^0 C_{O_2}^{0.4}$

[a] The photo-SCO was carried out at room temperature under photo-irradiation.
[b] The photo-SCO was carried out at 388 K under photo-irradiation.

3.6. Comparison of the reactivity of anatase TiO_2 between at room temperature and 388 K

The difference of the reactivity of anatase from room temperature to 388 K is discussed below. The rate-determining step is same (Step 5, Eq. (14)). Therefore, the rate equation can be expressed by Eq. (36). The value of k_5 of anatase TiO_2 at 388 K is about fifth as high as that of anatase at room temperature. The higher k_5 value at 388 K than at room temperature indicates that the reactivity of $NH_2^{\bullet}$–S with NO–S^- is enhanced by the increase in the reaction temperature. The concentrations of $NH_2^{\bullet}$–S and NO–S^- of anatase at 388 K were calculated by the substitution of k_5, r, K_3K_4 and $[O_2]$ into Eqs. (34) and (35). The obtained values of $[NH_2^{\bullet}–S]$ and $[NO–S^-]$ are listed in Table 1 (used values of r was 4.9×10^{-9} mol L^{-1} under the reaction condition of NH_3 = 1000 ppm and O_2 = 2% (8.90×10^{-4} mol L^{-1}) in Fig. 2(c1). The value of $[NO–S^-]$ is smaller than that of $[NH_2^{\bullet}–S]$. As the sum of $[NH_2^{\bullet}–S]$ and $[NO–S^-]$ is equal to the total amount of acid site ($[S]_0$), the acid site on TiO_2 would be also covered with NH_2 radical and NO species in the steady-state of the photo-SCO reaction at 388 K. Therefore, the ratio of $[NO–S^-]/[S]_0$ is the important factor for the photo-SCO activity according to Eq. (36). The value of $[NO–S^-]/[S]_0$ of anatase at 388 K was 0.33 and is closer to 0.5 than that of anatase at room temperature (0.26). The high $[NO–S^-]/[S]_0$ would be due to the enhancement of the reactivity of $NH_2^{\bullet}$–S with oxygen anion radical species in Eq. (13) by the increase in the reaction temperature because this process is the reaction of the surface species. Thus, we concluded that the increase in the reaction temperature enhances the photo-SCO activity without the change of the rate-determining step by the development of both k_5 and $[NO–S^-]/[S]_0$.

3.7. Activation energy of the photo-SCO over anatase TiO_2

Fig. 6 shows the Arrhenius plot of Fig. 4. The logarithm of N_2 formation showed a good linear relation to the reciprocal number and the obtained approximate line (shown in Fig. 6) was expressed as follows:

$$\ln r = \frac{-11.6(\pm0.3) - 2930(\pm110)}{T} \quad (41)$$

From Eq. (41), it was determined that the activation energy of the photo-SCO over anatase TiO_2 is 24.4 (±0.9) kJ mol^{-1}. The activation energy of the photo-SCO is much lower than that

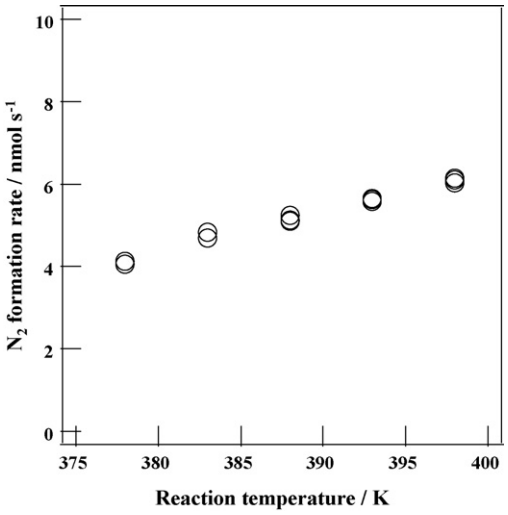

Fig. 4. The dependency of the N_2 formation rate on the reaction temperature in the photo-SCO over JRC-TiO*8 (used catalyst amount: 0.04 g, NH_3: 1000 ppm, O_2: 2%).

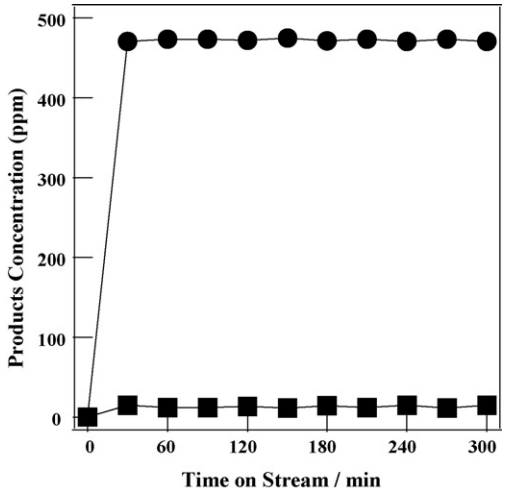

Fig. 5. Time course of the photo-SCO reaction over JRC-TIO-8, (●) outlet concentration of N_2, (■:) outlet concentration of N_2O. Reaction condition—NH_3: 1000 ppm, O_2: 2%, reaction temperature: 435 K, GHSV = 50,000 h^{-1}.

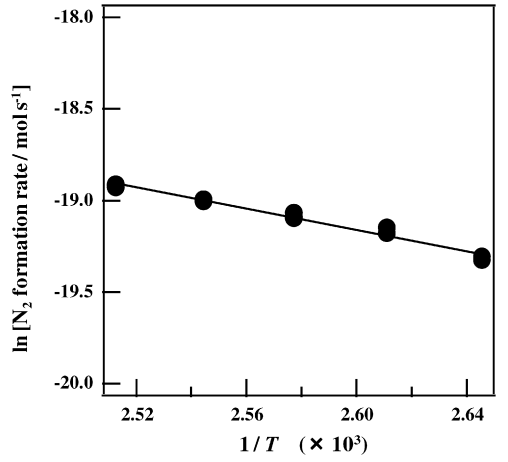

Fig. 6. Arrhenius plot of Fig. 4 (●) and the approximate line appeared in Eq. (41) (line).

of the conventional SCO over metal oxides. It was reported that the rate-determining step of the SCO reaction without photo-irradiation over metal oxide is Eq. (1) and that E_a of the SCO reaction is 76–139 kJ mol^{-1} [18–20]. The high E_a indicates that it is difficult to activate NH_3 by thermal energy. On the other hand, the activation of NH_3 (Eq. (11)) proceeds at wide range of the reaction temperature in the case of the photo-SCO because the photo-excitation is the driving force. This easy activation of NH_3 by light energy shifts the rate-determining step to another elementary step (Eq. (14)) having low activation energy. Therefore, the photo-SCO proceeds at room temperature with high activity.

4. Conclusion

The kinetic studies demonstrated that the photo-SCO depends on the concentration of O_2 over both anatse and rutile TiO_2. The experimental results are interpreted by assuming the steady-state approximation in the case that the rate-determining step is Step 4 (Eq. (14)) in Scheme 1. Thus, the validity of our proposed reaction mechanism (Scheme 1) is proved by the kinetics. The kinetic analysis reveals that the concentration of the surface NO–S^- species is important for the photo-SCO activity. The reason why anatase TiO_2 exhibits higher activity than rutile TiO_2 is that the concentration of NO–S^- species on anatase TiO_2 keeps high in the steady-state. This high NO–S^- concentration results from the strong oxidizabiliy of O_3 anion radical. The photo-SCO activity is enhanced by the increase in the reaction temperature. 100% NH_3 conversion and 94% N_2 selectivity were achieved at GHSV = 50,000 h^{-1} at 435 K. This enhancement of the activity by the increase in the reaction temperature is caused by the increase in both the rate constant (k_5) in the rate-determining step and the NO–S^- concentration. Moreover, the activation energy of the photo-SCO was estimated to be E_a = 24.4 kJ mol^{-1} by Arrhenius plot. The low activation energy allows for high SCO activity at low temperature.

Acknowledgement

S. Yamazoe is supported by a JSPS Research Fellowship for Young Scientists.

References

[1] R. Long, R. Yang, Chem. Commun. (2000) 1651.
[2] M. Yang, C. Wu, C. Zhang, H. He, Catal. Today 90 (2004) 263.
[3] L. Gang, B. Anderson, J. van Grondelle, R. van Santen, Appl. Catal. B 40 (2003) 101.
[4] E. Slavinskaya, S. Veniaminov, P. Notte, A. Ivanova, A. Boronin, Y. Chesalov, I. Polukhina, A. Noskov, J. Catal. 222 (2004) 129.
[5] L. Gang, B. Anderson, J. van Grondelle, R. van Santen, Catal. Today 61 (2000) 179.
[6] R. Long, R. Yang, J. Catal. 207 (2002) 158.
[7] R.W. Mccabe, T. Pignet, L.D. Schmidt, J. Catal. 32 (1974) 114.
[8] J.L. Gland, V.N. Korchak, J. Catal. 53 (1978) 9.
[9] A.C.M. van den Broek, J. van Grondelle, R.A. van Santen, J. Catal. 185 (1999) 297.
[10] M. Amblard, R. Burch, B.W.L. Southward, Catal. Today 59 (2000) 365.

[11] L. Lietti, G. Ramis, G. Busca, F. Bregani, P. Forzatti, Catal. Today 61 (2000) 187.
[12] S.A.C. Carabineiro, A.V. Matveev, V.V. Gorodetskii, B.E. Nieuwenhuys, Surf. Sci. 555 (2004) 83.
[13] Y.J. Li, J.N. Armor, Appl. Catal. B 13 (1997) 131.
[14] T. Curtin, F. O' Regan, C. Deconinck, N. Knuttle, B. Hodnett, Catal. Today 55 (2000) 189.
[15] L. Gang, J. van Grondelle, B. Anderson, R. van Santen, J. Catal. 186 (1999) 100.
[16] N. Sazonova, A. Simakov, T. Nikoro, G. Barannik, V. Lyakhova, V. Zheivot, Z. Ismagilov, H. Veringa, React. Kinet. Catal. Lett. 57 (1996) 71.
[17] W. Kijlstra, D. Brands, E. Poels, A. Bliek, J. Catal. 171 (1997) 208.
[18] N.I. Il'Chenko, G.I. Golodets, J. Catal. 39 (1975) 57.
[19] N.I. Il'Chenko, G.I. Golodets, J. Catal. 39 (1975) 73.
[20] Z.Y. Ding, L.X. Li, D. Wade, E.F. Gloyna, Ind. Eng. Chem. Res. 37 (1998) 1707.
[21] G. Ramis, L. Yi, G. Busca, M. Turco, E. Kotur, R.J. Willey, J. Catal. 157 (1995) 523.
[22] R.Q. Long, R.T. Yang, J. Catal. 201 (2001) 145.
[23] N. Cant, J.R. Cole, J. Catal. 134 (1992) 317.
[24] S. Yamazoe, T. Okumura, T. Tanaka, Catal. Today 120 (2007) 220.
[25] S. Yamazoe, T. Okumura, Y. Hitomi, T. Shishido, T. Tanaka, J. Phys. Chem. C 111 (2007) 11077.
[26] S. Yamazoe, T. Okumura, K. Teramura, T. Tanaka, Catal. Today 111 (2006) 266.
[27] K. Teramura, T. Tanaka, S. Yamazoe, K. Arakaki, T. Funabiki, Appl. Catal. B 53 (2004) 29.
[28] A.R. Gonzalez-Elipe, G. Munuera, J. Soria, J. Chem. Soc. Faraday I 75 (1979) 748.
[29] P. Meriaudeau, J.C. Vedrine, J. Chem. Soc. Faraday I 72 (1976) 472.
[30] H. Einaga, A. Ogata, S. Futamura, T. Ibusuki, Chem. Phys. Lett. 338 (2001) 303.
[31] S. Yamazoe, K. Teramura, Y. Hitomi, T. Shishido, T. Tanaka, J. Phys. Chem. C 111 (2007) 11077.
[32] H. Imahori, Y. Mori, Y. Matano, J. Photochem. Photobiol. C 4 (2003) 51.
[33] Y. Hu, S. Tsukiji, S. Shinkai, S. Oishi, I. Hamachi, J. Am. Chem. Soc. 122 (2000) 241.
[34] S.A.P. Merry, S. Kumazaki, Y. Tachibana, D.M. Joseph, G. Porter, K. Yoshihara, J. Barber, J.R. Durrant, D.R. Klug, J. Phys. Chem. 100 (1996) 10469.
[35] M. Okumura, J.M. Coronado, J. Soria, M. Haruta, J.C. Conesa, J. Catal. 203 (2001) 168.